

A Comparison Among Different Automatically Segmented Slabs to Assess Neovascular AMD using Swept Source OCT Angiography

Mariacristina Parravano¹, Enrico Borrelli^{2,3}, Riccardo Sacconi², Eliana Costanzo¹, Alessandro Marchese², Daniela Manca¹, Monica Varano¹, Francesco Bandello², and Giuseppe Querques²

¹ IRCCS - Fondazione Bietti, Rome, Italy.

² Ophthalmology Department, San Raffaele University Hospital, Milan, Italy.

³ Ophthalmology Clinic, Department of Medicine and Science of Ageing, University G. D'Annunzio Chieti-Pescara, Chieti, Italy.

Correspondence: Giuseppe Querques, Department of Ophthalmology, University Vita-Salute San Raffaele, Via Olgettina 60, Milan, Italy. e-mail: giuseppe.querques@hotmail.it

Received: 23 November 2018

Accepted: 9 January 2018

Published: 27 March 2019

Keywords: OCTA; neovascularization; neovascular; AMD

Citation: Parravano M, Borrelli E, Sacconi R, Costanzo E, Marchese A, Manca D, Varano M, Bandello F, Querques G. A comparison among different automatically segmented slabs to assess neovascular AMD using swept source OCT angiography. *Trans Vis Sci Tech.* 2019;8(2):8. <https://doi.org/10.1167/tvst.8.2.8>
Copyright 2019 The Authors

Purpose: We systematically compare the intermodality and interreader agreement in age-related macular degeneration (AMD)-associated neovascularization assessment for optical coherence tomography angiography (OCTA) images obtained using different slabs.

Methods: We collected data from 48 patients (50 eyes) with type 1 or 2 neovascularization (NV) and AMD. Subjects were imaged with a swept source (SS)-OCTA system. For each eye, three OCTA en face images generated from three different slabs were exported: (1) the outer retina to choriocapillaris (ORCC) image, (2) the choriocapillaris (CC) image, and (3) the retinal pigment epithelium (RPE)-RPE fit image. Each image was graded by two readers to assess interreader variability and a single image for each modality was used to assess the intermodality variability.

Results: In the assessment of type 1 NV, mean absolute interreader difference between measured NV areas was 0.19, 0.30, and 0.16 mm² for ORCC, CC, and RPE-RPE fit images, respectively. Similarly, the coefficient of repeatability (CR) and intraclass correlation coefficient (ICC) indicated that the RPE-RPE fit assessment was characterized by the highest interreader reproducibility. Type 1 NV size was 0.58 mm² (0.30–1.60 mm²) on ORCC images, 0.00 mm² (0.00–0.36 mm²) on CC images ($P = 0.002$ vs. ORCC), and 0.62 mm² (0.31–2.03 mm²) on RPE-RPE fit images ($P < 0.0001$ vs. CC, $P = 0.041$ vs. ORCC).

Conclusions: The RPE-RPE fit OCTA images have the highest interreader agreement and deliver larger measurements in type 1 lesions.

Translational Relevance: OCTA imaging may be used in ongoing trials of potential novel treatments for NV.

Introduction

Age-related macular degeneration (AMD) is the leading cause of irreversible central vision loss among older individuals in developed countries.¹ Early/intermediate AMD can progress to the late form of AMD notable for choroidal (Types 1 and 2) or retinal (Type 3) neovascularization, or geographic atrophy (GA). The presence of an exudative neovascular

lesion characterizes the “exudative neovascular form” of AMD.² Of note, neovascularization (NV) can be present without accumulation of fluid; this entity is termed “nonexudative neovascular AMD.”^{3–5}

Type 1 NV is the most common type of neovascular AMD and is characterized by pathologic angiogenesis, which mainly localizes between the retinal pigment epithelium (RPE) and Bruch's membrane.⁶ On the contrary, type 2 NV is characterized by the presence of pathologic vessels principally

confined in the subretinal space, and represents the least frequent phenotype of neovascular AMD, given that it accounts for 9% to 17% of all newly diagnosed cases.⁷

Optical coherence tomography angiography (OCTA) has proven to be an estimable imaging tool for assessment of neovascular AMD without the need for dye injection.⁸ Given that OCTA images are investigated mainly using en face visualization and acquired OCTA volumetric scans can be segmented at specific depths, visualization of types 1 and 2 NV may be obtained using different slabs. Although these slabs typically are manually outlined on the corresponding OCT cross-sectional B-scan images to include the whole neovascular membrane, this strategy often is labor intensive and has biases of manual grading. Thus, it has been assumed important to adopt standardized en face segmentation strategies to visualize and measure NV on OCTA images. Recently, the outer retina to choriocapillaris (ORCC) slab has been shown to be useful to assess types 1 and 2 NV.⁹ However, other automatically segmented slabs may be used to visualize NV on OCTA images.

We systematically compared the intermodality and interreader agreement in NV assessment for OCTA images obtained using different automatically segmented slabs. In details, assuming that type 1 NV is confined mainly between the RPE and Bruch's membrane, we investigated whether the RPE-RPE fit slab may represent a more suitable segmentation strategy for visualizing type 1 NV.

Methods

Study Participants

This multicenter, retrospective observational case series adhered to the tenets of the Declaration of Helsinki. Institutional review board (IRB) approval was obtained from the University Vita-Salute San Raffaele (Milan, Italy) and IRCCS - Fondazione Bietti (Rome, Italy).

In this study, subjects 50 years and older with treatment-naïve exudative neovascular AMD² were identified. All patients were imaged with the PLEX Elite 9000 device (Carl Zeiss Meditec, Inc., Dublin, CA) between 2017 and 2018. An IRB-approved informed consent was obtained from all patients. Moreover, all patients underwent a complete ophthalmologic examination, including measurement of best corrected visual acuity (BCVA), intraocular pressure (IOP), and dilated fundus examination.

Exclusion criteria for neovascular AMD eyes were previous ocular surgery or history of anti-vascular endothelial growth factor (VEGF) therapy, any evidence of type 3 NV in the enrolled eye, and poor quality images with a signal strength index (SSI) less than 6 or significant motion artifacts (seen as large dark lines on the en face angiogram).

Imaging

Patients underwent swept source (SS)-OCTA imaging using the PLEX Elite 9000 device (Carl Zeiss Meditec, Inc.), which uses a swept laser source with a central wavelength of 1050 nm and a bandwidth of 100 nm. This instrument has an axial resolution of approximately 5 μm and a lateral resolution estimated at approximately 14 μm . For each eye in the study, OCTA images using either the 3 \times 3- or 6 \times 6-mm scan pattern were acquired, according to the NV size and to include the whole neovascular lesion.

A fully-automated segmentation algorithm was used for the three-dimensional structural OCT data and applied to OCTA flow intensity with sum projection analyses, to obtain three different OCTA en face images: (1) the ORCC image that was obtained with a slab extended from the outer boundary of the outer plexiform layer (OPL) to 8 μm beneath Bruch's membrane, (2) the choriocapillaris (CC) image obtained using a slab 20 μm thick starting from Bruch's membrane, and (3) the RPE-RPE fit image that was visualized with a slab extended from the RPE to the RPE fit reference. The latter boundary is located at the outer limit of the ideal location of the RPE, where Bruch's membrane usually is placed. An automated algorithm to remove projections artifacts was used for each slab. Thus, the obtained en face images were exported as JPEG files with a resolution of 1024 \times 1024 pixels

Grading Protocol

First, all three OCTA en face images (ORCC, CC, and RPE-RPE fit) were opened in image analysis ImageJ software (National Institutes of Health [NIH], Bethesda, MD; available in the public domain at <http://imagej.nih.gov/ij/>).¹⁰ Then, two experienced graders (EB and EC) independently delineated the border of the NV lesions. Pixel counts from the outlined area were measured and were converted into area measurements. Graders were masked for the slab used to obtain the OCTA en face images and all images were mixed and randomly graded.

After grading of all the cases was completed, a

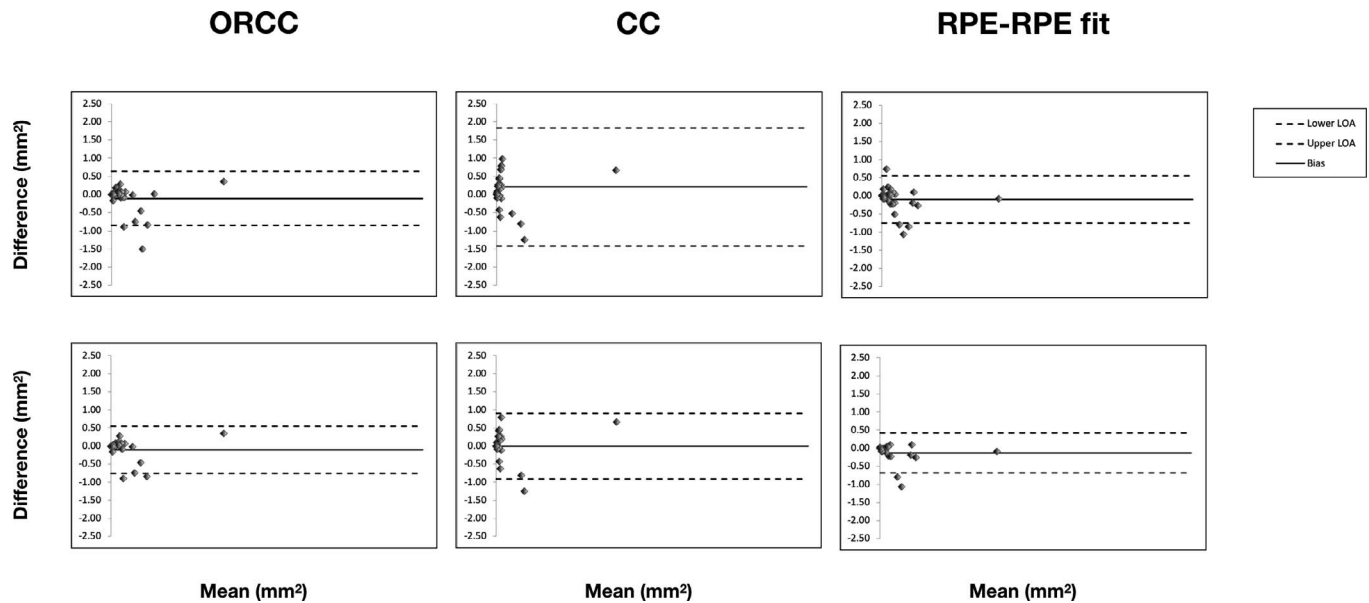


Figure 1. Bland-Altman graphs for interreader agreement considering the whole cohort (*upper line*) and exclusively enrolled eyes with type 1 NV (*lower line*). The Bland-Altman graphs (one for each slab investigated) show the measurement differences for the lesion area between two readers (*y-axis*) vs. mean of the two graders (*x-axis*). The *solid line* indicates mean difference (or bias) and the *dashed lines* indicate the 95% limits of agreement (upper and lower limits of agreement – LOA).

single graded image was used to assess the intermodality variability for NV size. Furthermore, these images were used to binarize and skeletonize the NV lesion, as shown previously.¹¹ Therefore, binarized and skeletonized images were used to investigate the NV perfusion and vessel length density, respectively. Thus, the perfusion density was calculated as a unitless proportion of the number of pixels over the threshold divided by the total number of pixels within the NV area on the binarized image. The vessel length density was defined as the total length of the perfused vasculature divided by the total number of pixels in the NV analyzed area on the skeletonized image.

Statistical Analysis

Statistical calculations were performed using Statistical Package for Social Sciences (version 20.0, SPSS, Inc., Chicago, IL). For each type of en face image (ORCC, CC, and RPE-RPE fit) mean absolute interreader difference, the intraclass correlation coefficient (ICC; two-way random, absolute agreement), and the 95% coefficient of repeatability (CR) were determined. For visualization of the level of agreement, Bland-Altman graphs were plotted.

Friedman's 2-way analysis of variance (ANOVA) nonparametric test was conducted to compare the graded NV area and NV perfusion and vessel length densities among the OCTA images, to assess the

intermodality variability. The chosen level of statistical significance was $P < 0.05$. The sample size of the study was tested to be proper for a mean difference between groups of almost 10%, a power of 80%, and type I error rate (α) of 5%.

Results

Characteristics of Patients Included in the Analysis

Of the 48 patients (50 eyes) with treatment-naïve exudative neovascular AMD who fulfilled inclusion criteria, six were excluded from the analysis because of poor scan quality. Of the 44 eyes (42 patients, 23 males) included in the analysis, 34 (77%) had type 1 NV, four (9%) type 2 NV, and six (14%) mixed types 1 and 2 NV. Mean age \pm standard deviation (SD) of the patients enrolled was 77.3 ± 6.2 years (range, 61–87 years).

Interreader Agreement

The level of agreement between graders is illustrated in the Bland-Altman plots (Fig. 1) and in Table 1. Mean absolute interreader difference between measured NV areas was 0.20, 0.46, and 0.20 mm² for ORCC, CC, and RPE-RPE fit images, respectively. The CR (the value below which the difference

Table 1. Comparison of Measurement From Three OCTA Images in the Whole Neovascular AMD Cohort

	ORCC	CC	RPE-RPE Fit
Mean absolute interreader difference, mm ²	0.20	0.46	0.20
CR, mm ²	0.75	1.61	0.66
ICC	0.973	0.890	0.980
NV area, mm ² , median (IQR)	0.73 (0.30–1.65)	0.00 (0.00–0.29)	0.65 (0.31–1.66)
NV perfusion density, median (IQR)	0.63 (0.54–0.69)	0.00 (0.00–0.54)	0.59 (0.50–0.68)
NV vessel length density, median (IQR)	0.07 (0.05–0.10)	0.00 (0.00–0.07)	0.07 (0.05–0.09)

FCR, 95% coefficient of repeatability.

between two measurements will lie in 95% of cases) was 0.75, 1.61, and 0.66 mm² for the for the ORCC-, CC-, and RPE-RPE fit-based grading, respectively. Likewise, the ICC (0.973, 0.890, and 0.980, respectively) indicated that ORCC- and RPE-RPE fit-based grading have the highest interreader agreements.

In a subanalysis considering only eyes with type 1 NV (Table 2), mean absolute interreader difference between measured NV areas was 0.19, 0.30, and 0.16 mm² for ORCC, CC, and RPE-RPE fit images, respectively. Similarly, the CR (0.65, 0.90, and 0.45 mm² for the ORCC-OCTA-, CC-OCTA-, and RPE-RPE fit-OCTA-based grading, respectively) and ICC (0.985, 0.976, and 0.989 for ORCC, CC, and RPE-RPE fit, respectively) indicated that the RPE-RPE fit assessment was characterized by the highest interreader reproducibility.

Intermodality Comparison

On ORCC images, 43 of 44 NV (98%) eyes were correctly identified (one type 1 NV was failed to be recognized). Graders were able to identify 18/44 NV (41%) eyes on CC images, since 17 type 1, three type 2, and six mixed NV cases were not properly distinguished. Finally, on RPE-RPE fit images, graders did identify 41 NV (93%) case and failed to identify 1 lesion for each NV type.

Median (interquartile range [IQR]) NV graded areas were 0.73 (0.30–1.65), 0.00 (0.00–0.29), and 0.65

(0.31–1.66) mm² for the ORCC, CC, and RPE-RPE fit images, respectively (Table 1). The NV area measurement was larger for ORCC than for CC images ($P < 0.0001$). Similarly, the RPE-RPE fit-based measurements were significantly larger than CC-based measurements ($P < 0.0001$). There was no significant difference in lesion area measurement between ORCC- and RPE-RPE fit-based grading ($P = 1.0$). The NV perfusion density was 0.63 (0.54–0.69), 0.00 (0.00–0.54; $P < .0001$ vs. ORCC), and 0.59 (0.50–0.68) on ORCC, CC, and RPE-RPE fit images ($P < 0.0001$ vs. CC, $P = 0.236$ vs. ORCC), respectively (Table 1). The NV vessel length density was 0.07 (0.05–0.10), 0.00 (0.00–0.07), and 0.07 (0.05–0.09) for the ORCC, CC, and RPE-RPE fit images, respectively ($P = 0.057$ ORCC vs. CC; $P = 0.017$ RPE-RPE fit vs. CC, and $P = 1.0$ RPE-RPE fit vs. ORCC; Table 1).

In a subanalysis that considered only eyes with type 1 NV (Table 2), the median (IQR) NV size was 0.58 (0.30–1.60), 0.00 (0.00–0.36; $P = 0.002$ vs. ORCC), and 0.62 (0.31–2.03) mm² on ORCC, CC, and RPE-RPE fit images ($P < 0.0001$ vs. CC, $P = 0.041$ vs. ORCC), respectively. The NV perfusion density (median = 0.62, IQR = 0.53–0.69 for ORCC images; median = 0.00, IQR = 0.00–0.55 for CC images; median = 0.59, IQR = 0.48–0.70 for RPE-RPE fit images) was lower for CC compared to ORCC ($P < 0.0001$) and RPE-RPE fit ($P = 0.001$) images. The NV perfusion density was slightly greater numerically in the RPE-RPE fit than in the ORCC

Table 2. Comparison of Measurement From Three OCTA Images in the Type 1 Neovascularization Cohort

	ORCC	CC	RPE-RPE fit
Mean absolute interreader difference, mm ²	0.19	0.30	0.16
CR, mm ²	0.65	0.90	0.45
ICC	0.985	0.976	0.989
NV area, mm ² , median (IQR)	0.58 (0.30–1.60)	0.00 (0.00–0.36)	0.62 (0.31–2.03)
NV perfusion density, median (IQR)	0.62 (0.53–0.69)	0.00 (0.00–0.55)	0.59 (0.48–0.70)
NV vessel length density, median (IQR)	0.07 (0.05–0.09)	0.00 (0.00–0.07)	0.07 (0.06–0.09)

images, although this difference did not reach statistical significance ($P = 0.372$). No differences in NV vessel length density were displayed among the three images (median = 0.07, IQR = 0.05–0.09 on ORCC; median = 0.00, IQR = 0.00–0.07 on CC; and median = 0.07, IQR = 0.06–0.09 on RPE-RPE fit).

Discussion

In this retrospective, cross-sectional study, we compared three OCTA en face images obtained using distinct automatically segmented slabs on visualizing and grading AMD-associated NVs. Overall, we observed that ORCC and RPE-RPE fit images provided an accurate and reproducible quantification of NV lesions. However, the RPE-RPE fit-based grading appears to be the most reliable and repeatable in assessing type 1 NV.

Numerous studies have evaluated eyes with AMD-associated NV using OCTA. Kuehlewein et al.¹² demonstrated that type 1 NV may be identified in 75% of the affected eyes as a highly organized vascular complex. Notably, the latter study demonstrated that type 1 NV may be characterized by two different patterns on OCTA images, including a “medusa” pattern in those cases with a branching pattern sprouting from the lesion core, and a “seafan” pattern when a branching pattern appears rising from one side of the lesion. Furthermore, OCTA was proved to have a high sensitivity for detecting type 1 NV, as assessed in a study comparing OCTA and fluorescein angiography (FA) sensitivities.¹³ In details, a detection sensitivity of 85.7% was demonstrated when OCTA and OCT data were combined. In contrast, a lower sensitivity was displayed with either OCTA or FA alone. Furthermore, type 1 NV was demonstrated to be significantly smaller on OCTA than indocyanine green angiography (ICGA) images, with this aspect suggesting that ICGA assessment may be affected by dye leakage.¹⁴ Type 2 NV has been characterized using OCTA and was demonstrated to appear either as a glomerulus-shaped lesion or as a medusa-shaped complex.^{15–17} The lesion visualized on OCTA corresponds topographically to a well-demarcated hyperfluorescent area in the early frames of FA images.¹⁵ Since OCTA provides a quantitative and qualitative assessment of the NV lesion, numerous studies have monitored the changes in these lesions occurring after anti-VEGF therapy.^{8,12,18–22} These studies proved that treatment reduces the density and perfusion of the smaller pathologic vessels, while larger vessels are mainly spared, causing a nonsignif-

icant reduction in the NV size after anti-VEGF treatment.

The technical characteristics of the OCTA device used to investigate neovascular AMD eyes were demonstrated to significantly affect the definition and quantification of NV. Novais et al.²³ compared spectral domain (SD)- and SS-OCTA instruments in the NV evaluation and proved a significant difference in measured NV area between these two systems. In details, the NV size was smaller when graded on the en face SD-OCTA images, which may be secondary to the fact that SD-OCT systems are more susceptible to sensitivity roll-off than SS-OCT systems.⁸

Taken together, these studies suggest that SS-OCTA may become an important imaging tool in the diagnosis and follow-up of patients with neovascular AMD. For this reason, it is unquestionably relevant to identify the best segmentation strategy to visualize NV on the OCTA en face images.

Our results showed an excellent interreader agreement in the ORCC- and RPE-RPE fit-based grading. By contrast, the ICC value was worse in the CC images. Moreover, even the CR, which is known to be independent of the average lesion size, was worse in the CC-based measurements. The reduced interreader agreement for the CC images was hypothesized to be secondary to the limited capability of this slab to incorporate the NV lesion, along with a complexity in distinguishing the pathologic vessels from the surrounding CC. In the post hoc analysis, which considered only eyes with type 1 NV, the highest interreader agreement was observed for RPE-RPE fit-based grading. This is most likely attributable to the sharper contrast at lesion boundaries in these images, as the NV lesion is not surrounded by normal CC vessels in the RPE-RPE fit OCTA image (Fig. 2).

We observed that CC-based lesion measurements were significantly smaller than ORCC- and RPE-RPE fit-based measurements, which is in agreement with our interpretation that the CC slab is incapacitated to visualize the whole NV, even taking into consideration only type 1 NV. Moreover, while the CC image had a lower sensitivity in the NV detection, we found that ORCC and RPE-RPE fit slabs have the same sensitivity (33/34 eyes, 97%) for detecting type 1 NV using OCTA en face images. Of note, in the post-hoc analysis analyzing type 1 NV, we observed larger NV area measurement from RPE-RPE fit compared to ORCC images. This aspect may be partially due to the fact that ORCC images include the CC plexus. The CC vessels may partially mask the NV margin and the

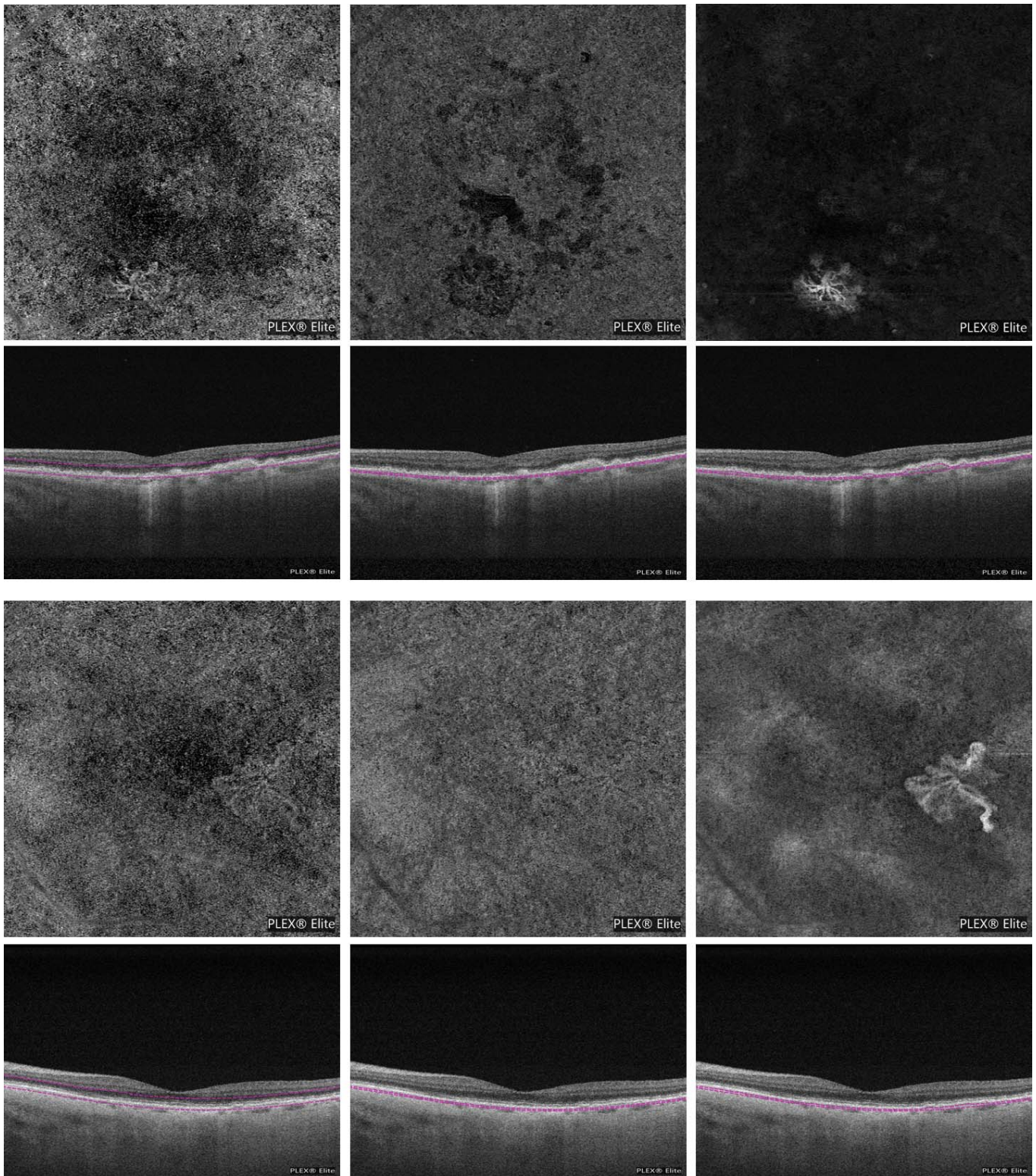


Figure 2. En face OCTA images (*first and third lines*) and corresponding cross-sectional OCT images (*second and fourth lines, respectively*) showing the slab used to obtain the en face images from 2 eyes (one for each pair of lines) affected by exudative neovascular AMD with type 1 NV. The ORCC en face image (*left*) shows flow within a neovascular lesion. This lesion is poorly visible in the CC en face image (*middle*). The RPE-RPE fit en face image (*right*) appears superior in showing the NV lesion, even compared to the ORCC image, since a larger amount of lesion is displayed, as well as an higher contrast between the neovascular and perilesional region is evident.

grader presumably was not certain as to whether such peripheral regions should be included as NV (Fig. 2).

Of note, though not statistically significant, we observed a trend for a slightly higher NV perfusion density for RPE-RPE fit compared to ORCC images. This aspect may be partially due to an improved visualization of the smaller pathologic neovessels using the RPE-RPE fit slab. Indeed, since OCTA images were obtained with sum projection analyses, a thicker slab may result in a reduced visualization of the smaller vessels, assuming that this analysis projection creates an image that is the sum of the slices in the slab. However, assuming that these differences did not reach statistical significance and that we did not find differences in the NV vessel length density, this aspect needs further investigations to be discussed properly.

Our study has some limitations that should be considered when assessing our findings. First, the sample size of the cohort is relatively small, which reduces the power of our analysis. In particular, we were not powered to evaluate for differences between the ORCC and RPE-RPE fit assessments of type 2 NV. However, given that type 2 NV is located mainly in the subretinal space, it is supposable that the ORCC slab may confer a better visualization of this kind of neovascularization. Second, we did use 3×3 - and 6×6 -mm images. However, we used a SS-OCTA system, which was demonstrated to have a greater consistency in lesion area measurements across different scan patterns.²⁴ Finally, image quality may have impacted on perfusion and vessel length density measurements. However, poor quality images with an SSI less than 6 or significant motion artifacts were not included in our analysis.

In summary, using SS-OCTA en face images obtained using the ORCC and RPE-RPE fit slabs allowed an accurate and reproducible quantification of NV in AMD patients. The RPE-RPE fit OCTA images have the highest interreader agreement in the measurement of type 1 lesion size. Furthermore, these images delivered larger measurements of type 1 NV compared to ORCC images. Regardless, the potential of RPE-RPE fit slab to evaluate type 1 lesions warrants further study, and may be of particular relevance given the many ongoing trials of potential novel treatments for NV.

Acknowledgments

Supported in part by the Italian Ministry of Health and Fondazione Roma.

Disclosures: **M. Parravano**, Allergan (S), Bayer (S); Novartis (S); **E. Borrelli**, None; **R. Sacconi**, None; **E. Costanzo**, None; **A. Marchese**, None; **D. Manca**, None; **M. Varano**, Allergan (S), Bayer (S); Novartis (S); Sifi (S); **F. Bandello**, Allergan (S), Alimera (S), Bayer (S), Farmila-Thea (S), Schering Pharma (S), Sanofi-Aventis (S), Novagali (S), Pharma (S), Hoffmann-La Roche (S), Genetech (S), Novartis (S); **G. Querques**, Allergan (S), Alimera (S), Amgen (S), Bayer (S), KHB (S), Novartis (S), Roche (S), Sandoz (S), Zeiss (S); Allergan (C), Alimera (C), Bausch and Lomb (C), Bayer (C), Heidelberg (C), Novartis (C), Zeiss (C)

References

1. Friedman DS, O'Colmain BJ, Muñoz B, et al. Prevalence of age-related macular degeneration in the United States. *Arch Ophthalmol*. 2004;122:564–572.
2. Ferris FL, Wilkinson CP, Bird A, et al. Clinical classification of age-related macular degeneration. *Ophthalmology*. 2013;120:844–851.
3. Roisman L, Zhang Q, Wang RK, et al. Optical coherence tomography angiography of asymptomatic neovascularization in intermediate age-related macular degeneration. *Ophthalmology*. 2016;123:1309–1319.
4. de Oliveira Dias JR, Zhang Q, Garcia JMB, et al. Natural history of subclinical neovascularization in nonexudative age-related macular degeneration using swept-source OCT angiography. *Ophthalmology*. 2018;125:255–266.
5. Carnevali A, Cicinelli MV, Capuano V, et al. Optical coherence tomography angiography: a useful tool for diagnosis of treatment-naïve quiescent choroidal neovascularization. *Am J Ophthalmol*. 2016;169:189–198.
6. Grossniklaus HE, Gass JD. Clinicopathologic correlations of surgically excised type 1 and type 2 submacular choroidal neovascular membranes. *Am J Ophthalmol*. 1998;126:59–69.
7. Jung JJ, Chen CY, Mrejen S, et al. The incidence of neovascular subtypes in newly diagnosed neovascular age-related macular degeneration. *Am J Ophthalmol*. 2014;158:769–779.
8. Borrelli E, Sarraf D, Freund KB, Sadda SR. OCT angiography and evaluation of the choroid and choroidal vascular disorders. *Prog Retin Eye Res*. 2018;67:30–55.

9. Zhang Q, Chen CL, Chu Z, et al. Automated quantitation of choroidal neovascularization: a comparison study between spectral-domain and swept-source OCT angiograms. *Invest Ophthalmol Vis Sci.* 2017;58:1506–1513.
10. Schneider CA, Rasband WS, Eliceiri KW. NIH Image to ImageJ: 25 years of image analysis. *Nat Methods.* 2012;9:671–675.
11. Al-Sheikh M, Iafe NA, Phasukkijwatana N, Sadda SR, Sarraf D. Biomarkers of neovascular activity in age-related macular degeneration using OCT angiography. *Retina.* 2018;33:220–230.
12. Kuehlewein L, Bansal M, Lenis TL, et al. Optical coherence tomography angiography of type 1 neovascularization in age-related macular degeneration. *Am J Ophthalmol.* 2015;160:739–748.
13. Inoue M, Jung JJ, Balaratnasingam C, et al. A comparison between optical coherence tomography angiography and fluorescein angiography for the imaging of type 1 neovascularization. *Invest Ophthalmology Vis Sci.* 2016;57:OCT314–OCT323.
14. Costanzo E, Miere A, Querques G, Capuano V, Jung C, Souied EH. Type 1 Choroidal neovascularization lesion size: indocyanine green angiography versus optical coherence tomography angiography. *Invest Ophthalmol Vis Sci.* 2016;57:OCT307–OCT313.
15. El Ameen A, Cohen SY, Semoun O, et al. Type 2 neovascularization secondary to age-related macular degeneration imaged by optical coherence tomography angiography. *Retina.* 2015;35:2212–2218.
16. Willoughby a S, Ying GS, Toth C a, et al. Subretinal hyperreflective material in the comparison of age-related macular degeneration treatments trials. *Ophthalmology.* 2015;122:1846–53.e5.
17. Dansingani KK, Tan ACS, Gilani F, et al. Subretinal hyperreflective material imaged with optical coherence tomography angiography. *Am J Ophthalmol.* 2016;169:235–248.
18. Huang D, Jia Y, Rispoli M, Tan O, Lumbroso B. Optical coherence tomography angiography of time course of choroidal neovascularization in response to anti-angiogenic treatment. *Retina.* 2015;35:2260–2264.
19. Mastropasqua L, Toto L, Borrelli E, Carpineto P, Di Antonio L, Mastropasqua R. Optical coherence tomography angiography assessment of vascular effects occurring after aflibercept intravitreal injections in treatment-naive patients with wet age-related macular degeneration. *Retina.* 2017;37:247–256.
20. Coscas G, Lupidi M, Coscas F, Français C, Cagini C, Souied EH. Optical coherence tomography angiography during follow-up: qualitative and quantitative analysis of mixed type I and II choroidal neovascularization after vascular endothelial growth factor trap therapy. *Ophthalmic Res.* 2015;54:57–63.
21. Kuehlewein L, Sadda SR, Sarraf D. OCT angiography and sequential quantitative analysis of type 2 neovascularization after ranibizumab therapy. *Eye.* 2015;29:932–935.
22. Parravano M, Querques L, Scarinci F, et al. Optical coherence tomography angiography in treated type 2 neovascularization undergoing monthly anti-VEGF treatment. *Acta Ophthalmol.* 2017;95:e425–426.
23. Novais EA, Adhi M, Moulton EM, et al. Choroidal neovascularization analyzed on ultrahigh-speed swept-source optical coherence tomography angiography compared to spectral-domain optical coherence tomography angiography. *Am J Ophthalmol.* 2016;164:80–88.
24. Zheng F, Zhang Q, Motulsky EH, et al. Comparison of neovascular lesion area measurements from different swept-source OCT angiographic scan patterns in age-related macular degeneration. *Invest Ophthalmol Vis Sci.* 2017;58:5098–5104.